Nucleon electric dipole moment from the θ term with lattice chiral fermions

Jian Liang,[1,2,*] Andrei Alexandru,[3] Terrence Draper,[4] Keh-Fei Liu,[4] Bigeng Wang,[4] Gen Wang,[5] and Yi-Bo Yang[6,7,8,9]

(χQCD Collaboration)

[1]*Key Laboratory of Atomic and Subatomic Structure and Quantum Control (MOE), Guangdong Basic Research Center of Excellence for Structure and Fundamental Interactions of Matter, Institute of Quantum Matter, South China Normal University, Guangzhou 510006, China*
[2]*Guangdong-Hong Kong Joint Laboratory of Quantum Matter, Guangdong Provincial Key Laboratory of Nuclear Science, Southern Nuclear Science Computing Center, South China Normal University, Guangzhou 510006, China*
[3]*Department of Physics, The George Washington University, Washington, District of Columbia 20052, USA*
[4]*Department of Physics and Astronomy, University of Kentucky, Lexington, Kentucky 40506, USA*
[5]*Aix-Marseille Université, Université de Toulon, CNRS, CPT, 7332, Marseille, France*
[6]*CAS Key Laboratory of Theoretical Physics, Institute of Theoretical Physics, Chinese Academy of Sciences, Beijing 100190, China*
[7]*School of Fundamental Physics and Mathematical Sciences, Hangzhou Institute for Advanced Study, UCAS, Hangzhou 310024, China*
[8]*International Centre for Theoretical Physics Asia-Pacific, Beijing/Hangzhou, China*
[9]*University of Chinese Academy of Sciences, School of Physical Sciences, Beijing 100049, China*

(Received 7 February 2023; accepted 13 October 2023; published 27 November 2023)

We calculate the nucleon electric dipole moment (EDM) from the θ term with overlap fermions on three domain wall lattices with different sea pion masses at lattice spacing 0.11 fm. Due to the chiral symmetry conserved by the overlap fermions, we have well-defined topological charge and chiral limit for the EDM. Thus, the chiral extrapolation can be carried out reliably at nonzero lattice spacings. We use three to four different partially quenched valence pion masses for each sea pion mass and find that the EDM dependence on the valence and sea pion masses behaves oppositely, which can be described by partially quenched chiral perturbation theory. With the help of the cluster decomposition error reduction technique, we determine the neutron and proton EDM at the physical pion mass to be $d_n = -0.00148(14)(31)\bar{\theta}\ \mathrm{e}\cdot\mathrm{fm}$ and $d_p = 0.0038(11)(8)\bar{\theta}\ \mathrm{e}\cdot\mathrm{fm}$. This work is a clear demonstration of the advantages of using chiral fermions in the nucleon EDM calculation and paves the road to future precise studies of the strong CP violation effects.

DOI: 10.1103/PhysRevD.108.094512

I. INTRODUCTION

Symmetries and their breaking are essential topics in modern physics, among which the discrete symmetries C (charge conjugation), P (parity), and T (time reversal) are of special importance. This is partially because the violation of the combined C and P symmetries is one of the three Sakharov conditions [1] that are necessary to give rise to the baryon asymmetry of the universe (BAU). However, despite the great success of the standard model (SM), the weak baryogenesis mechanism from the CP violation ($\not{C}\not{P}$) within the SM contributes negligibly (∼16 orders of magnitude smaller than the observed BAU [2–6]). This poses a hint that, besides the possible θ term in QCD, there could exist beyond-standard-model (BSM) sources of $\not{C}\not{P}$ and thus the study of $\not{C}\not{P}$ plays an important role in the efforts of searching for BSM physics.

The electric dipole moment of nucleons (NEDM) serves as an important observable to study $\not{C}\not{P}$. The first experimental upper limit on the neutron EDM (nEDM) was given in 1957 [7] as $\sim 10^{-20}\ \mathrm{e}\cdot\mathrm{cm}$. During the past 60 years of experiments, this upper limit has been improved by six orders of magnitude. The most recent experimental result of the nEDM is $0.0(1.1)(0.2)\times 10^{-26}\ \mathrm{e}\cdot\mathrm{cm}$ [8], which is still around five orders of magnitude larger than the contribution

*jianliang@scnu.edu.cn

that can be offered by the weak $\mathcal{CP}$ phase. Currently, several experiments are aiming at improving the limit down to 10^{-28} e · cm in the next ∼10 years. This still leaves plenty of room for the study of $\mathcal{CP}$ from BSM interactions and the QCD θ term.

As a reliable nonperturbative method for solving the strong interaction, lattice QCD provides us the possibility of studying the nucleon EDM from first principles and with both the statistical and systematic uncertainties under control. To be specific, lattice QCD can be used to calculate the ratio between the neutron and proton EDM induced by strong $\mathcal{CP}$ and the parameter $\bar{\theta}$, which is the most crucial theoretical input to determine $\bar{\theta}$ from experiments.

Many lattice calculations have been carried out on this topic. However, there was a watershed in 2017 when it was pointed out [9] that all the previous lattice calculations, e.g., [10–14], used a wrongly defined $\mathcal{CP}$ form factor such that all of those old results need a correction. Although the fixing is numerically straightforward, none of the previous lattice calculations gives statistically significant results after the fixing, leaving a great challenge to the lattice community. Since then, several attempts [15–18] have been made to tackle the problem, but the signal-to-noise ratios of the new results are still not satisfying, and no calculation performed directly at the physical point gives nonzero results.

A possibility to bypass this difficulty is to perform the computations with several heavier pion masses and extrapolate to the physical point. However, only with chiral fermions can a correct chiral limit be reached at finite lattice spacings. Otherwise, extrapolating to the continuum limit for each pion mass becomes an inevitable prior step before a reliable chiral extrapolation, which complicates the calculation and potentially leads to hard-to-control systematic uncertainties. The best result, so far, of this approach, using clover fermions, obtained a 2σ signal [16]. One could also carry out the continuum limit using simulations with physical pion masses directly, but the signal can be even more noisy.

In this article, we demonstrate that using chiral fermions to extrapolate to the physical point from heavier pion masses is the most efficient choice to study NEDM on the lattice at the current stage. We employ three gauge ensembles with different sea pion masses ranging from ∼300 to ∼600 MeV and we use three to four valence pion masses on each lattice. Therefore, we can study both the valence and sea pion mass dependence of the NEDM and better control the chiral extrapolation. The results we obtain at the physical pion mass are $d_n = -0.00148(14)(31)\bar{\theta}$ e · fm and $d_p = 0.0038(11)(8)\bar{\theta}$ e · fm for neutron and proton, respectively.

More details of the nucleon EDM and θ term will be provided in Secs. II and III presents the simulation setup used in this work. Numerical results taking advantage of the cluster decomposition error reduction (CDER) technique for the disconnected insertion [19] are shown in Sec. IV, with the discussion on the systematic uncertainties in Sec. V. Eventually a brief summary is given in Sec. VI.

II. NUCLEON EDM AND THE θ TERM

The QCD Lagrangian in Euclidean space with the θ term reads (detailed conventions can be found in the Appendix),

$$\mathcal{L}^E = \bar{\psi}(\not{D}^E + m_q)\psi + \frac{1}{2}\mathrm{Tr}\left[F^E_{\mu\nu}F^{E,\mu\nu} - i\bar{\theta}\frac{g^2}{8\pi^2}F^E_{\mu\nu}\tilde{F}^{E,\mu\nu}\right], \tag{1}$$

where $\tilde{F}^{E,\mu\nu} = \epsilon^{\mu\nu\rho\sigma}F^E_{\rho\sigma}$. The effective parameter is $\bar{\theta} = \theta + \frac{1}{N_f}\mathrm{ArgDet}[M]$, where θ is the original coefficient of the θ term and M is the quark mass matrix generated by the spontaneous breaking of $SU(2) \times U(1)$ in the electroweak sector. For simplicity, we will not distinguish θ and $\bar{\theta}$ in the following content. A crucial point is that, if $\mathrm{Det}[M] = 0$, the phase of the $U_A(1)$ transformation is arbitrary, which means one can always find a chiral rotation that lets $\bar{\theta} = 0$, leaving no net effect of $\mathcal{CP}$. This indicates a zero NEDM in the chiral limit [20], which poses a very strong constraint in the chiral extrapolation numerically. However, as mentioned before, for lattice fermions which violate the chiral symmetry this constraint cannot be used at finite lattice spacing.

Given that θ is small, one can expand the theta term in the action in the path integral and obtain the correlation functions and matrix elements to the leading order in θ as ${}_\theta\langle\ldots\rangle_\theta = \langle\ldots\rangle + i\theta\langle\ldots Q_t\rangle$, where $|0\rangle_\theta$ denotes the vacuum with the θ term (namely, the θ vacuum), and $Q_t = \int d^4x q_t(x) \equiv \frac{g^2}{16\pi^2}\int d^4x \mathrm{Tr}[F^E_{\mu\nu}(x)\tilde{F}^{E,\mu\nu}(x)]$ is the topological charge of the gauge field. Based on this expansion, the $\mathcal{CP}$ electromagnetic (EM) form factor $F_3(q^2)$ can be extracted from normal and Q_t weighted nucleon matrix elements with initial momentum $p_i = (m, \vec{0})$ and final momentum $p_f = (E_f, \vec{q})$ as

$$\begin{aligned} F_3(q^2) &= \frac{2m}{E_f + m}\left\{\frac{2E_f}{q_i}\frac{\mathrm{Tr}[\Gamma_i M_4^{(3)Q}]}{\mathrm{Tr}[\Gamma_e M^{(2)}]} - \alpha^1 G_E(q^2)\right\}, \\ G_E(q^2) &= \frac{2E_f}{E_f + m}\frac{\mathrm{Tr}[\Gamma_e M_4^{(3)}]}{\mathrm{Tr}[\Gamma_e M^{(2)}]}, \quad \alpha^1 = \frac{\mathrm{Tr}[\gamma_5 M^{(2)Q}]}{2\mathrm{Tr}[\Gamma_e M^{(2)}]}, \end{aligned} \tag{2}$$

where the matrix elements are

$$\begin{aligned} M^{(2)} &= \langle N(p_f)|N(p_i)\rangle, \\ M^{(3)}_\mu &= \langle N(p_f)|V_\mu|N(p_i)\rangle, \\ M^{(2)Q} &= \langle N(p_f)|Q_t|N(p_i)\rangle, \\ M^{(3)Q}_\mu &= \langle N(p_f)|Q_t V_\mu|N(p_i)\rangle, \end{aligned} \tag{3}$$

with V_μ being the EM current operator, $\Gamma_e = \frac{1+\gamma_4}{2}$ the unpolarized spin projector, $\Gamma_i = -i\gamma_5\gamma_i\Gamma_e$ the polarized projector along the ith direction, $q^2 = (p_f - p_i)^2 = -Q^2$

the momentum transfer, and q_i the nonzero component of the momentum transfer. The above formalism is the same for both neutron and proton. In the end, the nucleon EDM can be extracted from the $\mathcal{CP}$ form factor $F_3(q^2)$ in the forward limit for neutron and proton respectively using

$$d_{n/p} = \frac{F_{3,n/p}(q^2 \to 0)}{2m}\theta. \tag{4}$$

An interesting fact, as seen in Eq. (2), is that the neutron $\mathcal{CP}$ form factor at the zero momentum transfer limit, $F_{3,n}(0)$ has no $\mathcal{CP}$ angle α^1 dependence since $G_{E,n}(0) = 0$.

III. NUMERICAL SETUP

This study is carried out on three $(2+1)$-flavor RBC/UKQCD gauge ensembles of domain wall fermions [21] with the same lattice spacing 0.1105(3) fm and lattice volume $24^3 \times 64$ but different sea quark masses. Using the overlap fermion action [22] on the hypercubic (HYP) smeared [23] gauge links, multiple partially quenched valence quark masses (as listed in Table I with other parameters) are calculated utilizing the multimass inversion algorithm; thus both the sea and valence pion mass dependencies of NEDM can be studied and the chiral extrapolation can be more reliable.

Generally, the simplest implementation of overlap fermions can be $\mathcal{O}(100)$ times more costly compared to the traditional Wilson-like discretized fermion actions. To improve the computational efficiency, 12-12-12 grid sources with Z_3-noise and Gaussian smearing are placed at $t_{\rm src} = 0$ and $t_{\rm src} = 32$ in one inversion with randomly chosen spatial positions of the grid original point on different configurations, and low-mode substitution (LMS) [24] is applied to suppress the statistical contamination between different source positions. We also use the stochastic sandwich method (SSM) [25] with LMS to make the cost of using multiple nucleon sinks be additive instead of multiplicative. We use 8 sets of source noises and 16 sets of sink noises (for each of the source-sink separations $6a$, $7a$, and $8a$) to improve the statistics. Five nonzero momentum transfers are calculated such that we can reliably do the q^2 extrapolation to get $F_3(0)$; the details of the q^2 extrapolation will be given in Sec. V.

In this study, we use overlap fermions as valence quarks. The overlap Dirac operator $D_{\rm ov}$ satisfies the Ginsparg-Wilson relation, which ensures the lattice version of chiral symmetry at finite lattice spacing a. Moreover, since the modified quark field $\hat{\psi} = (1 - 1/2D_{\rm ov})\psi$ is used for the chirally regulated current operators and interpolating fields, the effective quark propagator is then $1/(D_c + m_q)$, where m_q is the current quark mass and $D_c = D_{\rm ov}/(1 - 1/2D_{\rm ov})$ anticommutes with γ_5, i.e., $\{D_c, \gamma_5\} = 0$ [26]. This is the same form as in the continuum and the eigenvalues of D_c are purely imaginary. Actually, it has been shown that all the current algebra is satisfied with overlap fermions at finite a. In particular, the anomalous Ward identity (AWI) has been proven by Peter Hasenfratz [23] for $D_{\rm ov}$ with chiral axial vector current. And we have also shown numerically [27] that the normalization factor Z_A obtained from the axial Ward identity in the isovector case is the same (within error) as the one from the AWI in the singlet case.

TABLE I. Parameters of the RBC/UKQCD ensembles with $L \times T = 24^3 \times 64$ at 0.1105(3) fm [21]; label, sea and valence pion masses, nucleon mass with unitary quark mass, and the number of configurations.

Label	$m_{\pi,s}$ (MeV)	$m_{\pi,v}$ (MeV)				$m_N(m_{\pi,s})$ (GeV)	$N_{\rm cfg}$
24I005	339	282	321	348	389	1.14	805
24I010	432		426	519	600	1.25	508
24I020	560		432	525	606	1.30	552

Geometrically, the θ term is related to the topological charge of the gauge field $Q_t = \int d^4x q_t(x) \equiv \frac{g^2}{32\pi^2}\int d^4x F^E_{\mu\nu}(x)\tilde{F}^{E,\mu\nu}(x)$. Usually, the $F\tilde{F}$ definition of the topological charge with unsmeared gauge fields suffers from large UV effects and cannot give integer total topological charge values on the lattice (a review on this topic can be found in [28]). One way to solve the problem is to use the gradient flow to smooth the gauge fields and to get renormalized topological charges [29–31]. Since we are using a lattice chiral fermion, we have an alternative way to obtain the topological charge. According to the Atiyah-Singer index theorem, the topological charge equals the numerical difference between the left-handed zero modes of $D_{\rm ov}$ and the right-handed zero modes, that is, $Q_t = n_- - n_+$, which ensures integer topological charge on each configuration with no additional renormalization. This definition is theoretically the same as the definition from the overlap Dirac operator

$$Q_t = \frac{1}{2}{\rm Tr}[\gamma_5 D_{\rm ov}] = -{\rm Tr}\left[\gamma_5\left(1 - \frac{D_{\rm ov}}{2}\right)\right], \tag{5}$$

where the trace over all color, spin, and space-time indices of $D_{\rm ov}$ can be estimated through noise sources. And this $D_{\rm ov}$ definition can also be used to define the topological charge density $q_t(x)$. The topological charge term is essential in the nEDM calculation and the overlap definition reduces the subtleties in the evaluation of the topological charges, which is another benefit of using chiral fermions.

It is interesting to note the difference between topological charges from the overlap definition and those from the gluonic definition with long enough gradient flow until integer topological charge values are reached. We find that, as shown in Fig. 1, the total topological charge on

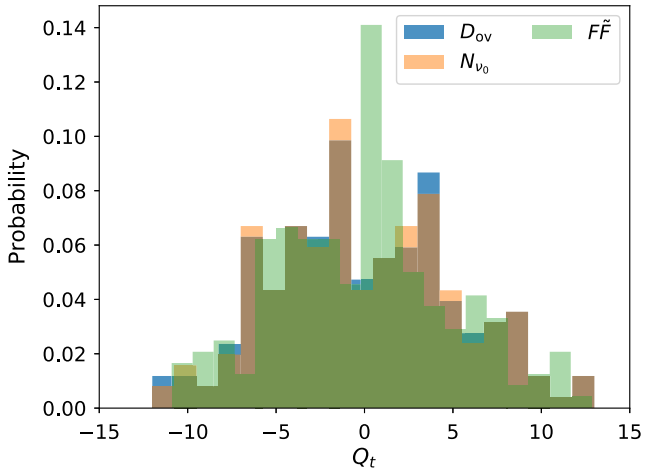

FIG. 1. Topological charge distributions over gauge configurations with different definitions. The distribution with label N_{ν_0} corresponds to the topological charges from counting the zero modes, which should be the same as the one with label $D_{\rm ov}$. The nuanced difference between them comes from the fact that $D_{\rm ov}$ is estimated by noise and has statistical fluctuations. The distribution with label $F\tilde{F}$ corresponds to that using the gluonic definition with $t_f = 4a^2$. The brown color is the overlay of orange and blue.

individual configurations with the gluonic definition is not necessarily the same as the one with the overlap definition. This is actually natural as they involve different regulations. However, the topological charge distributions over different gauge configurations in a given ensemble are similar. All the distributions are approximately symmetric with central value at around zero, and it seems the gluonic definition gives more zero charges. Now, a further question is whether they will lead to consistent physical results at finite lattice spacing.

For the purpose of checking physical results, we calculate the topological susceptibility on the same lattice

$$\chi_t = \frac{1}{V}\langle Q_t^2 \rangle. \tag{6}$$

The upper panel of Fig. 2 plots the fourth root of the topological susceptibilities $\chi_t^{1/4}$ from the $F\tilde{F}$ definition with different flow time and the overlap definition as a function of pion mass. It shows that at large flow time t_f, the value of the topological susceptibility from the gluonic definition tends to approach that from the overlap definition. However, it is found that, even at $t_f = 6a^2$, the χ_t value from the gluonic definition is still around 10% higher than that from the overlap definition, and this discrepancy roughly remains unchanged for the three different pion masses we use. Although there is a gentle trend that the central values will be closer as the flow time t_f is larger

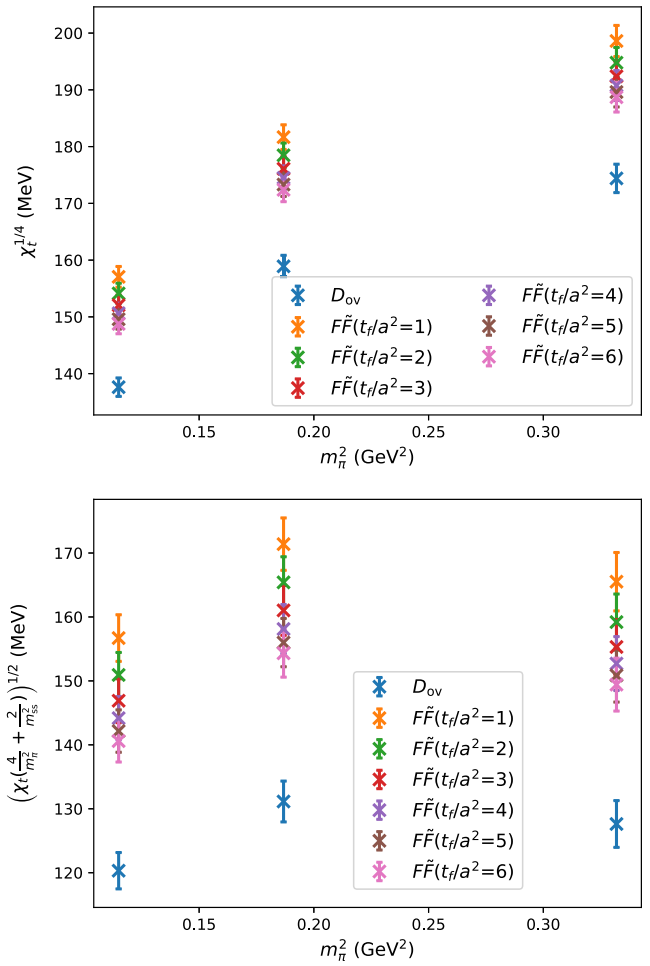

FIG. 2. The fourth root of the topological susceptibilities $\chi_t^{1/4}$ (upper panel) and $(\chi_t(\frac{4}{m_{\pi,l}^2}+\frac{2}{m_{\pi,s}^2}))^{1/2}$ (lower panel) from the $F\tilde{F}$ definition with different flow time and the overlap definition are plotted as a function of pion mass.

still, for the study at only one lattice spacing, it is hard to justify a precise choice of t_f that is large enough. The difference can be attributed to the $\mathcal{O}(a^2)$ discretization error. To further verify which definition is optimal to use in this study, we plot $(\chi_t(\frac{4}{m_{\pi,l}^2}+\frac{2}{m_{\pi,s}^2}))^{1/2}$ in the lower panel of Fig. 2, which should give the pion decay constant f in the leading-order $(2+1)$-flavor chiral perturbation theory, since

$$\chi_t = \frac{f^2}{\frac{4}{m_{\pi,l}^2}+\frac{2}{m_{\pi,s}^2}}. \tag{7}$$

One can see that the values from the overlap definition are closer to the physical value. This demonstrates that the overlap definition of the topological charge has smaller discretization error and is more reasonable to use in the numerical calculation as well as the chiral extrapolation. Another conclusion that can be drawn here is that the

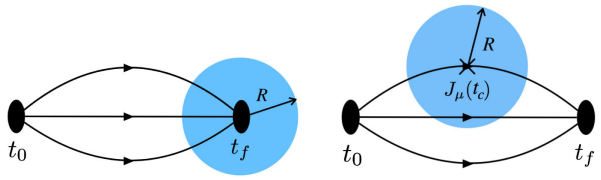

FIG. 3. Illustration of the CDER technique used when computing the correlation functions with the local topological charge summed inside the sphere with radius R.

specific topological charge value on each single configuration has not much effect on the physical correlations; only the distribution matters.

IV. CDER IMPROVEMENT AND RESULTS

To further suppress the statistical uncertainty of $M^{(2)Q}$ and $M^{(3)Q}$, we take advantage of CDER for the disconnected insertion [19]. As illustrated in Fig. 3, we write the total topological charge as the summation of the local charge density $q_t(x)$ derived from the overlap operator [32,33] as $q_t(x) = \frac{1}{2}\mathrm{Tr}[\gamma_5 D_{\mathrm{ov}}(x,x)]$, where the trace is over the color-spin indices, and convert the two-point function weighted with the total topological charge Q_t into a summation of the three-point functions involving $q_t(x)$

$$G^{(2)Q} = \sum_{\vec{x}} \left\langle \sum_r q_t(x+r)\chi(x)\bar{\chi}(t_0,\mathcal{G}) \right\rangle, \tag{8}$$

where χ is the nucleon interpolating operator, $\mathcal{G}$ denotes the source grid, and $x = (t_f, \vec{x})$. We then use the cluster decomposition property to limit the sum to a range commensurate with the correlation length

$$\begin{aligned} G^{(2)Q} &\sim \sum_{\vec{x}} \left\langle \sum_r^{|r|<R} q_t(x+r)\chi(x)\bar{\chi}(t_0,\mathcal{G}) \right\rangle \\ &\sim M^{(2)Q} + \mathcal{O}(e^{-\delta m t_f}, e^{-m_\eta R}), \end{aligned} \tag{9}$$

which reduces the variance by a volume factor [19]. In Eq. (9), R is the four-dimensional truncated size of the topological operator, δm is the effective mass gap between the nucleon and its excited states, and m_η is the mass of the pseudoscalar meson η.

Similarly, the three-point function with Q_t can be converted into a four-point function with $q_t(x)$

$$\begin{aligned} G^{(3)Q} &\sim \sum_{\vec{x}\vec{y}} e^{-i\vec{q}(\vec{x}-\vec{y})} \left\langle \chi(x) \sum_r^{|r|<R} q_t(y+r) J_\mu(y) \bar{\chi}(t_0,\mathcal{G}) \right\rangle \\ &\sim M^{(3)Q} + \mathcal{O}(e^{-\delta m(t_c-t_0)}, e^{-\delta E(\vec{q})(t_f-t_c)}, e^{-m_\eta R}), \end{aligned} \tag{10}$$

where $y = (t_c, \vec{y})$, and $\delta E(\vec{q})$ is the energy gap of the nucleon and its excited states with 3-momentum $\vec{q}$ at the sink. Using Eqs. (9) and (10), the $\mathcal{CP}$ form factor F_3 can be calculated as a function of cutoff R. Due to the cluster decomposition principle, operators far enough separated have exponentially small correlation. When the distance between operators is larger than the correlation length $\sim 1/m_\eta$, the signal falls below the noise while the errors still accumulate in the disconnected insertions [19]. So we bind the topological charge to the sink of the nucleon in the three-point functions or to the inserted currents in the four-point function to see if a proper cutoff R exists, such that the physics is not altered while the errors can be reduced.

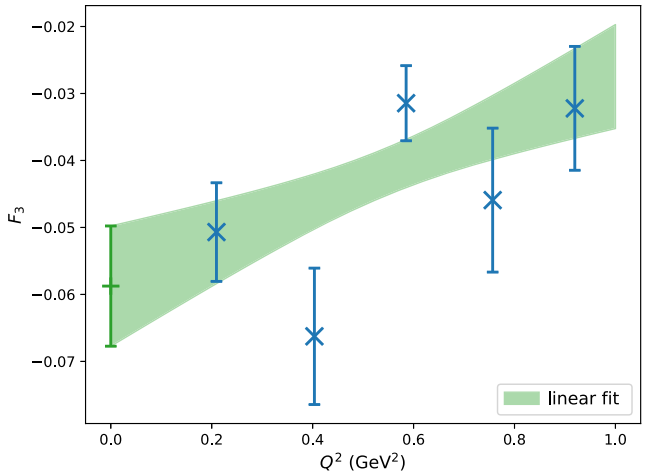

FIG. 4. The cutoff dependence of $F_{3,n}(Q^2 = 0.2\ \mathrm{GeV}^2)$ with different $m_{\pi,v}$ and $m_{\pi,s} = 339$ MeV. We can see that the value saturates at $R \sim 9a$.

Then we do the two-state fit to eliminate the excited-state contamination of nucleon matrix elements at each value of R, and obtain $F_3(Q^2)$ as a function of R. The corresponding systematic uncertainty is estimated to be the difference between the value from the two-state fits and that from single-exponential fits using only the middle point at different separations. Taking $F_{3,n}(Q^2 = 0.2\ \mathrm{GeV}^2)$ at $m_{\pi,s} = 339$ MeV and different $m_{\pi,v}$ as an example (shown in Fig. 4), the central value starts to saturate at around $R = 9a \sim 2/m_\eta$ as expected. Since the R dependence for different pion masses are similar, we choose $R_c = 9a$ as our optimal cutoff in the neutron case. For the proton, we use $R_c = 10a$. The systematic uncertainty of this cutoff will be discussed in detail in Sec. V.

Benefited from CDER, the data points of $F_{3,n}(Q^2)$ show a non-vanishing Q^2 dependence as shown in Fig 5 for the case of $m_{\pi,v} \sim m_{\pi,s} = 340$ MeV, while there is no significant deviation from a linear shape. Thus, we use a linear fit for the extrapolation to $Q^2 = 0$, and estimate the corresponding systematic uncertainty to be the difference between the extrapolated value and the data value with the smallest Q^2.

After the $Q^2 \to 0$ extrapolation, the final chiral extrapolation of the neutron EDM is shown in the upper panel of Fig. 6 with both valence and sea pion mass dependencies. We observe that the partially quenched data behave

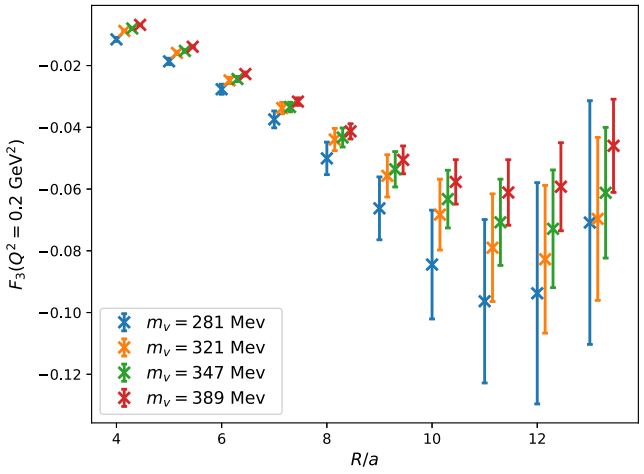

FIG. 5. The Q^2 dependence of $F_{3,n}$ with $m_{\pi,v} \sim m_{\pi,s} = 339\,\mathrm{MeV}$. The green band shows a linear fit in Q^2.

differently from those with unitary points in the lower panel. The former tend to move away from zero as the valence quark mass decreases. Using the overlap fermion allows us to fit our data with the partially quenched chiral perturbation form [34] at finite lattice spacing,

$$d_{n,p} = c_{1,n/p} m_{\pi,s}^2 \log\left(\frac{m_{\pi,v}^2}{m_N^2}\right) + c_{2,n/p} m_{\pi,s}^2 + c_{3,n/p}(m_{\pi,v}^2 - m_{\pi,s}^2), \tag{11}$$

where $c_{1,2,3,n/p}$ are free parameters. Our lattice data are well-fitted to the above form with $\chi^2/\mathrm{d.o.f.} = 1.2$ using correlated fittings, and our numerical results suggest that the different valence and sea quark mass dependence is consistent with the chiral perturbation expression. It is also interesting to point out that the chiral log term is crucial to ensure that the NEDM approaches zero in the chiral limit of both the valence and sea quark masses. With the zero NEDM constraint at the chiral limit, our interpolated result for neutron is $d_n = -0.00148(14)\bar{\theta}\ \mathrm{e}\cdot\mathrm{fm}$, where the statistical uncertainty is less than 10%. This is quite an improvement from the 2σ statistical error in Ref. [16].

We also carry out another chiral extrapolation using only the unitary pion mass points, as shown in the lower panel of Fig. 6. It gives $d_n = -0.00142(20)\bar{\theta}\ \mathrm{e}\cdot\mathrm{fm}$, which is consistent with the prediction using partially quenched data points but with larger statistical uncertainty. We take the difference between the extrapolated results with and without partially quenched data points as an estimation of the systematic uncertainty in the chiral extrapolation.

The proton EDM and its systematic uncertainties can be obtained with a similar procedure and the result is shown in

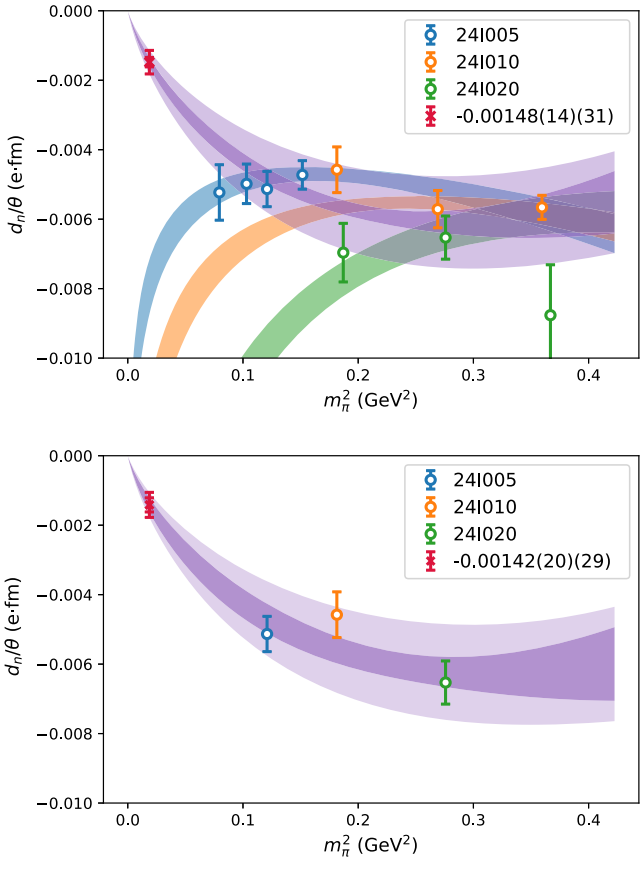

FIG. 6. The chiral extrapolation of d_n/θ on both the sea and valence quark masses (upper panel) and on only the unitary points (lower panel).

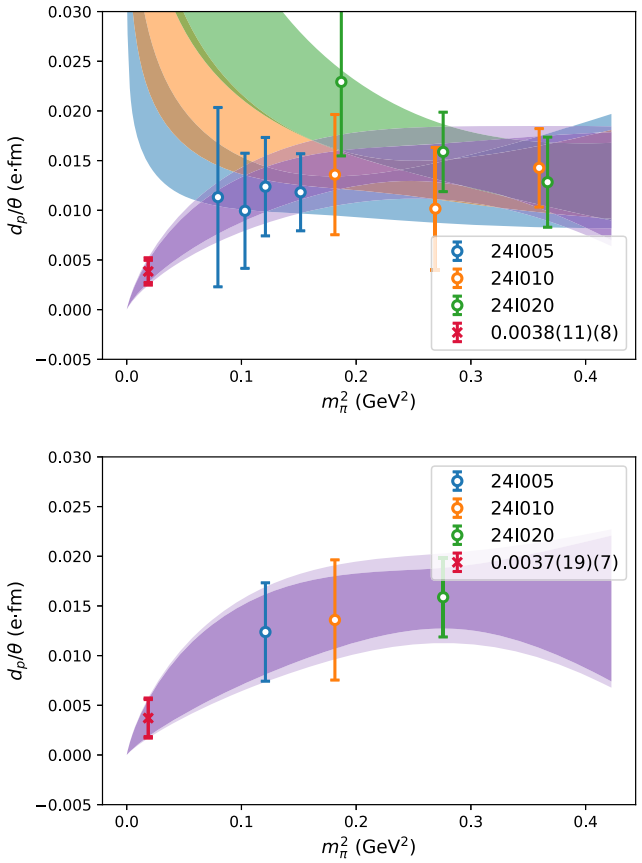

FIG. 7. The same as Fig. 6 but for the proton case.

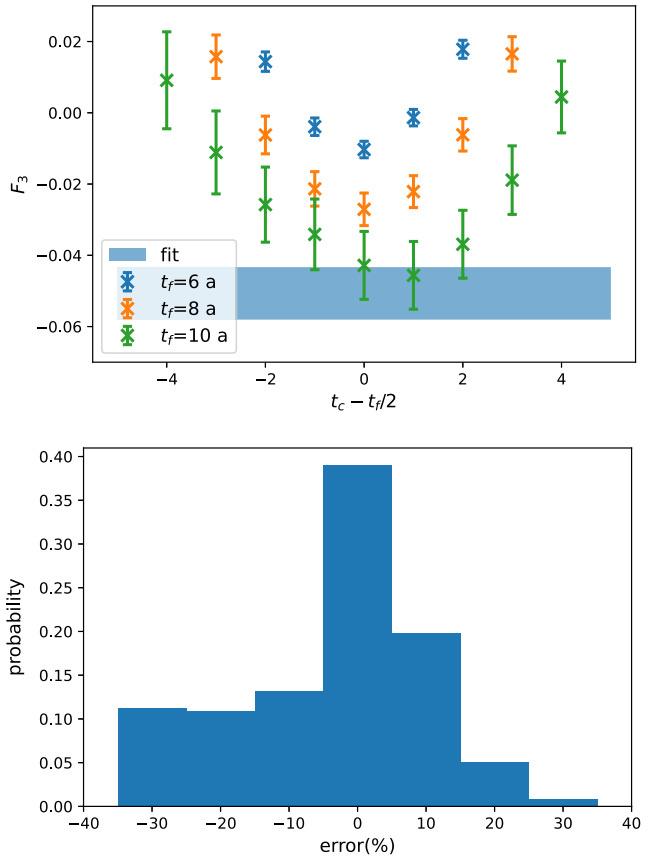

FIG. 8. An example of a two-state fit of $F_{3,n}$ with $Q^2 = 0.2$ GeV^2, $R = 9a$ and $m_{\pi,v} \sim m_{\pi,s} = 339$ MeV (upper panel) and the systematic uncertainty distribution over different momentum transfers, CDER cutoffs and pion masses (lower panel).

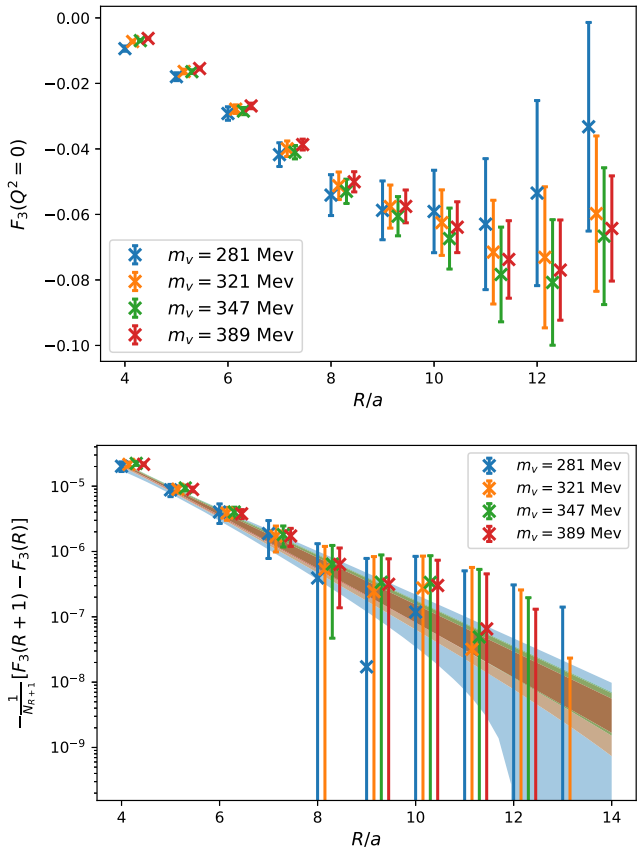

FIG. 9. Upper panel: The cutoff dependence of $F_{3,n}(Q^2 = 0)$ with different $m_{\pi,v}$ and $m_{\pi,s} = 339$ MeV. Lower panel: The correlation in terms of the 4D distance r between the topological charge operator and the current operator. Different colors are for different pion masses.

Fig. 7. More detailed discussion on the systematic uncertainty estimation will be presented in the next section.

V. SUMMARY ON THE SYSTEMATIC UNCERTAINTIES

In this study, the main sources of systematic uncertainties are the two-state fits of the three-point (four-point) function to two-point function ratios, the momentum extrapolation, the use of the CDER technique, the final chiral extrapolation, and the finite lattice spacing effect.

1) Two-state fit: The systematic uncertainty from the two-state fit is estimated by the difference between the two-state fitted values and the results from single-exponential fits using only the middle point at different separations. Usually, one compares the two-state fits results and the values of the middle data point at the largest separations to estimate the systematic uncertainty. In our case, since we are using relatively small source-sink separations, we fit the middle points to a simplified form $C_0 + C_1 e^{-mt_f}$ to account for the excited-state effect on different separations t_f. Then, we consider the distribution of the difference between the two-state results and C_0's (as shown in the lower panel of Fig. 8), and take the 1σ width (68% probability) to be the final systematic uncertainty, which is determined to be 13%.

2) CDER technique: The systematic uncertainty due to the use of the CDER technique is a crucial one. The key idea of CDER is that operators have finite correlation length and going beyond the correlation length results in only noise rather than signal. In our case, the topological charge operator is summed up to a cutoff R with the center being at the position of the EM current. We can have an optimal cutoff to have saturated signal and improved statistical error. The upper panel of Fig. 9 shows the d_n dependence on the cutoff R. We do observe that, after $R \geq 9a$, the central values do not change (within errors) while the errors are getting larger. The lower panel of Fig. 9 shows the difference of d_n normalized by the number of equivalent R's

$$\frac{1}{N_{R+1}}[d_n(R+1) - d_n(R)], \tag{12}$$

which is in fact the correlation in terms of the 4-D distance r between the topological charge operator and the current operator, since

$$d_n(R) \sim \sum_{|r|<R} \langle N|q(x+r)J_\mu(x)|N'\rangle, \tag{13}$$

where $\langle N|q(x+r)J_\mu(x)|N'\rangle$ denotes the nucleon matrix element that encodes the correlation. This panel demonstrates that the correlation decays exponentially and there is indeed a finite correlation length. The optimal cutoff is chosen to be $R_0 = 9a$. The systematic error can obtained by two ways. One is to take the difference between the value at $R_0 = 9a$ and the constant fitted value after that cutoff. From data such as that in the left panel the systematic uncertainty is estimated to be ∼10–15% in this way. The other way is to fit the correlation to an exponential form first, and then put the fitted correlation in the summation $d_n(R) \sim \sum_{|r|>R_0} \langle q(0+r)J_\mu(0)\rangle$ to estimate the contribution from the truncated tail. In this way, with the correlation

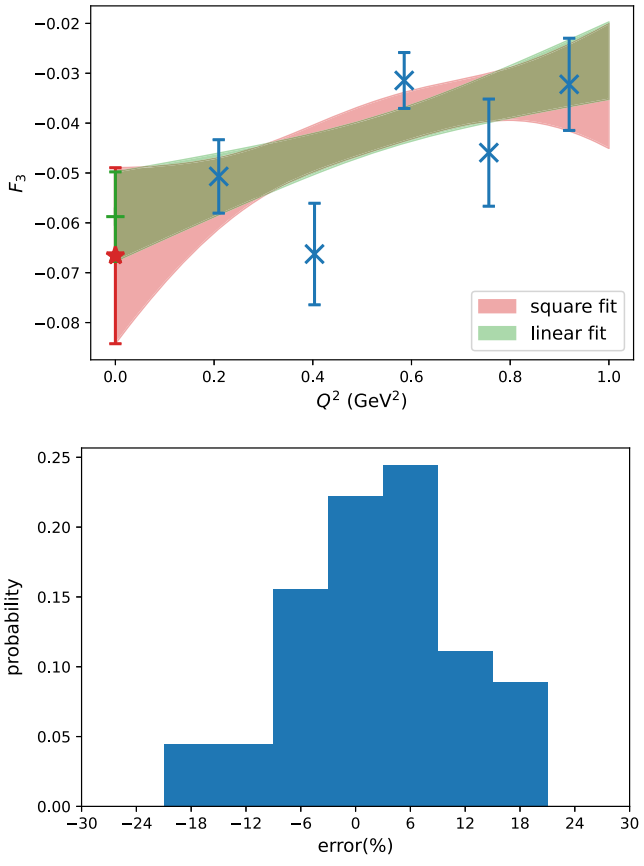

FIG. 10. An example of momentum transfer extrapolation of $F_{3,n}$ with $R = 9a$ and $m_{\pi,v} \sim m_{\pi,s} = 339$ MeV (upper panel) and the systematic uncertainty distribution over CDER cutoffs and pion masses lower panel). In the upper panel, blue points are lattice data and the green band shows a linear fit in Q^2 while the red band shows the fit with an additional Q^4 term.

data such as that in the lower panel of Fig. 9, the corresponding systematic uncertainty is estimated to be ∼10%. So the two methods give consistent systematic uncertainties and we choose ∼12% to be our final estimation.

3) Momentum extrapolation: Considering the systematic uncertainty from the momentum extrapolation, although we have five momentum transfers, the data points show no significant deviation from a linear shape due to the large uncertainties, so we use a linear fit for the extrapolation and estimate the corresponding systematic uncertainty to be the difference between the extrapolated value and the data value with the smallest momentum transfer. Similar to the two-state fit case, the systematic uncertainty is estimated to be 10% by taking the 1σ width of the error distribution shown in the upper panel of Fig. 10. We can also estimate this systematic uncertainty by the difference between the extrapolated results with or without a Q^4 term, which is also 10% of the central value and consistent with the present estimate.

4) Chiral extrapolation: For the systematic uncertainty from the chiral extrapolation, we take the difference of the extrapolations with and without partially quenched data points to be our estimation. As shown in Fig. 6 (the chiral fits for neutron) and Fig. 7 (that for proton), the difference is around 3%. The small systematic uncertainty of chiral interpolation is understandable since the chiral limit provides a very strong constraint to the interpolation.

The total systematic uncertainty is found to be 21%, which is simply calculated by quadrature from all the systematic uncertainties.

VI. SUMMARY

We calculate the nucleon electric dipole moment with overlap fermions on 3 domain wall lattices at lattice spacing 0.11 fm. Since the overlap fermion preserves chiral symmetry, we have well-defined topological charge and the chiral extrapolation is carried out reliably without the need of doing continuum extrapolations first. We have in total three sea pion masses and ten partially quenched valence pion masses in the chiral fitting and find that the EDM dependence on the sea and valence pion masses behaves oppositely, as expected from partially quenched chiral perturbation theory.

With the help of the CDER technique, we determine the neutron and proton EDM at the physical pion mass point to be $d_n = -0.00148(14)(31)\bar{\theta}$ e · fm and $d_p = 0.0038(11)(8)\bar{\theta}$ e · fm, respectively. The two uncertainties are the statistical uncertainty and the total systematic uncertainty from the excited-state contamination, the CDER cutoff, and the Q^2 and chiral extrapolations. By using the most recent experimental upper limit of d_n, our results indicate that $\bar{\theta} < 10^{-10}$. This work demonstrates the advantage of using chiral fermions in the NEDM

calculation and paves the road to future precise studies of the strong $\mathcal{CP}$ effects.

ACKNOWLEDGMENTS

J. L. is supported by Guangdong Major Project of Basic and Applied Basic Research under Grant No. 2020B0301030008, Science and Technology Program of Guangzhou under Grant No. 2019050001, and the Natural Science Foundation of China (NSFC) under Grant No. 12175073 and No. 12222503. T. D. and K. L. are supported in part by the Office of Science of the U.S. Department of Energy under Grant No. DE-SC0013065 (T. D. and K. L.) and No. DE-AC05-06OR23177 (K. L.), which is within the framework of the TMD Topical Collaboration. Y. Y. is supported in part by the Strategic Priority Research Program of Chinese Academy of Sciences, Grants No. XDB34030303 and No. XDPB15, NSFC under Grant No. 12293062, and also a NSFC-DFG joint grant under Grant No. 12061131006 and SCHA 458/22. G. W. is supported by the French National Research Agency under the Contract No. ANR-20-CE31-0016. A. A. is supported in part by U.S. DOE Grant No. DE-FG02-95ER40907. This research used resources of the Oak Ridge Leadership Computing Facility at the Oak Ridge National Laboratory, which is supported by the Office of Science of the U.S. Department of Energy under Contract No. DE-AC05-00OR22725. This work used Stampede time under the Extreme Science and Engineering Discovery Environment (XSEDE), which is supported by National Science Foundation Grant No. ACI-1053575. We also used resources on Frontera at Texas Advanced Computing Center (TACC). The analysis work is partially done on the supercomputing system in the Southern Nuclear Science Computing Center (SNSC). We also thank the National Energy Research Scientific Computing Center (NERSC) for providing HPC resources that have contributed to the research results reported within this paper. We acknowledge the facilities of the USQCD Collaboration used for this research in part, which are funded by the Office of Science of the U.S. Department of Energy.

APPENDIX A: CONVENTIONS AND FORMALISM

In this part of the appendix, we list our notations and conventions in a very detailed manner, which we think is quite worthwhile since the final sign of EDM depends directly on the conventions used.

1. Gamma matrices

First, for the gamma matrices in Minkowski space, we use

$$\{\gamma_\mu, \gamma_\nu\} = 2\eta_{\mu\nu}, \tag{A1}$$

where $\eta_{\mu\nu} = (+,-,-,-)$ is the corresponding metric tensor. Similarly, we have, for the Euclidean ones,

$$\{\gamma_\mu^E, \gamma_\nu^E\} = 2\eta_{\mu\nu}^E, \tag{A2}$$

with $\eta_{\mu\nu}^E = (+,+,+,+)$. Our choice is to let $\gamma_4^E = \gamma^0$ while $\gamma_i^E = -i\gamma^i$. For the momentum we have $p_4^E = iE = ip^0$ and $p_i^E = p^i$, this definition ensures $\not{p} = \gamma_0 p^0 + \gamma_i p^i = -i\gamma_4^E p_4^E - i\gamma_i^E p_i^E = -i\not{p}^E$.

Then, with the above definitions, we come to the following conventions of the spinors

$$u\bar{u} = \frac{\not{p} + m}{2m}, \qquad u^E\bar{u}^E = \frac{-i\not{p}^E + m}{2m}, \tag{A3}$$

and we define

$$\sigma_{\mu\nu} = \frac{i}{2}[\gamma_\mu, \gamma_\nu], \qquad \sigma_{\mu\nu}^E = \frac{1}{2i}[\gamma_\mu^E, \gamma_\nu^E]. \tag{A4}$$

in our notations.

2. QCD Lagrangian with the θ term

The Minkowski QCD Lagrangian reads

$$\begin{aligned}\mathcal{L} &= \bar{\psi}(i\not{D} - m)\psi - \frac{1}{4}F_{\mu\nu}^a F_a^{\mu\nu} \\ &= \bar{\psi}(i\not{D} - m)\psi - \frac{1}{2}\mathrm{Tr}[F_{\mu\nu}F^{\mu\nu}],\end{aligned} \tag{A5}$$

where the covariant derivative is $D_\mu \equiv \partial_\mu - igA_\mu$ with a minus sign in front of A_μ. Along with this convention, we use

$$F_{\mu\nu} \equiv \frac{1}{-ig}[D_\mu, D_\nu] = \partial_\mu A_\nu - \partial_\nu A_\mu - ig[A_\mu, A_\nu]. \tag{A6}$$

To have the QCD Lagrangian in Euclidean space, we first notice $\partial^0 = i\partial_4^E$ and $\partial^i = -\partial_i^E$, and for the gauge fields, the conversion is the same as that of p^E and p,

$$A_4^E = iA^0, \qquad A_i^E = A^i. \tag{A7}$$

Combining the above relations, we come to

$$D^0 = \frac{\partial}{\partial x_0} - igA^0 \to i\left(\frac{\partial}{\partial x_4^E} + igA_4^E\right) \equiv iD_4^E, \tag{A8}$$

and

$$D^i = \frac{\partial}{\partial x_i} - igA^i \to -\left(\frac{\partial}{\partial x_i^E} + igA_i^E\right) \equiv -D_i^E. \tag{A9}$$

Plugging in the conversions of the gamma matrices, we have

$$iD^0\gamma_0 + iD^i\gamma_i - m = -D_4^E\gamma_4^E - D_i^E\gamma_i^E - m. \tag{A10}$$

The Minkowski field tensor satisfies

$$F_{\mu\nu}F^{\mu\nu} = 2\sum F_{0i}F^{0i} + 2\sum_{i<j} F_{ij}F^{ij} = -2E^2 + 2B^2, \tag{A11}$$

where $E^i = E_i = F_{0i} = -F^{0i}$, and $B^i = -\frac{1}{2}\epsilon^{ijk}F_{jk} = B_i = -\frac{1}{2}\epsilon_{ijk}F^{jk}$. It is easy to check that

$$E^i = -iE_i^E, \qquad B^i = -B_i^E, \tag{A12}$$

and such that

$$F_{\mu\nu}^E F^{E,\mu\nu} = 2[(E^E)^2 + (B^E)^2] = F_{\mu\nu}F^{\mu\nu}. \tag{A13}$$

Then, we finally reach the form of the QCD Lagrangian in Euclidean space

$$\mathcal{L}^E = \bar{\psi}(\not{D}^E + m)\psi + \frac{1}{2}\mathrm{Tr}[F_{\mu\nu}^E F^{E,\mu\nu}]. \tag{A14}$$

When the θ term is taken into consideration, in Minkowski space, we have $\mathcal{L} \to \mathcal{L} + \mathcal{L}_\theta$ and

$$\mathcal{L}_\theta = \bar{\theta}\frac{g^2}{32\pi^2}F_{\mu\nu}^a\tilde{F}_a^{\mu\nu} = \bar{\theta}\frac{g^2}{16\pi^2}\mathrm{Tr}[F_{\mu\nu}\tilde{F}^{\mu\nu}] \equiv \bar{\theta}q_t \tag{A15}$$

where $\tilde{F}^{\mu\nu} = \epsilon^{\mu\nu\rho\sigma}F_{\rho\sigma}$ and q_t is the topological charge density. Based on the above conversions, we have

$$\begin{aligned} F_{\mu\nu}\tilde{F}^{\mu\nu} &= 2\sum F_{0i}\tilde{F}^{0i} + 2\sum_{i<j} F_{ij}\tilde{F}^{ij} = -8E\cdot B, \\ F_{\mu\nu}^E\tilde{F}^{E,\mu\nu} &= 2\sum F_{0i}^E\tilde{F}^{E,0i} + 2\sum_{i<j} F_{ij}^E\tilde{F}^{E,ij} = 8iE\cdot B, \end{aligned} \tag{A16}$$

and in the end

$$\begin{aligned} \mathcal{L}^E + \mathcal{L}_\theta^E = \bar{\psi}(\not{D}^E + m)\psi + \frac{1}{2}\mathrm{Tr}[F_{\mu\nu}^E F^{E,\mu\nu}] \\ - i\bar{\theta}\frac{g^2}{16\pi^2}\mathrm{Tr}[F_{\mu\nu}^E\tilde{F}^{E,\mu\nu}]. \end{aligned} \tag{A17}$$

3. Spinors under the θ vacuum

Now we have determined the Lagrangian in Euclidean space. In the following part of the appendix, we will work in the Euclidean space and omit the superscript ^{E} unless otherwise specified.

After the θ term is plugged in, the P and CP symmetries are broken. The normal Dirac equation and spinor definition should be modified. The new Dirac equation reads

$$[-i\not{p} - m^\theta e^{-i\alpha(\theta)\gamma_5}]u^\theta = \bar{u}^\theta[-i\not{p} - m^\theta e^{-i\alpha(\theta)\gamma_5}] = 0, \tag{A18}$$

where the superscript θ denotes quantities under the θ vacuum and $\alpha(\theta)$ is an unknown function of θ. Up to terms linear in θ (due to the smallness of θ), we have, for example,

$$[-i\not{p} - m(1 + f_m^1\theta)(1 - i\alpha^1\theta\gamma_5)](1 + f_u^1\theta)u = 0, \tag{A19}$$

where f_m^1, α^1, and f_u^1 are expansion coefficients. Subtracting the normal Dirac equation, we get

$$-m(f_m^1 - i\alpha^1\gamma_5)u + [-i\not{p} - m]f_u^1 u = 0. \tag{A20}$$

Since the nucleon mass has no leading θ correction [35]

$$m^\theta = m + \mathcal{O}(\theta^2), \tag{A21}$$

the new spinors can be expressed as

$$u^\theta = e^{i\alpha^1\theta\gamma_5}u \tag{A22}$$

and

$$\bar{u}^\theta = \bar{u}e^{i\alpha^1\theta\gamma_5}, \tag{A23}$$

such that we have

$$u^\theta(p)\bar{u}^\theta(p) = \frac{-i\not{p} + me^{i2\alpha^1\gamma_5\theta}}{2m}. \tag{A24}$$

Also, we define the overlapping factor

$$\langle 0|\chi|N\rangle = Zu, \tag{A25}$$

where χ is the nucleon interpolating field operator and $|N\rangle$ is the corresponding nucleon state. Then, under the θ vacuum we define

$${}_\theta\langle 0|\chi|N\rangle_\theta = Z^\theta u^\theta. \tag{A26}$$

Similarly, we have

$$Z^\theta = Z + \mathcal{O}(\theta^2). \tag{A27}$$

4. Form factors

In Minkowski space, we use the following electromagnetic form factor decomposition

$$\langle N'|\bar{\psi}\gamma_\mu\psi|N\rangle = \bar{u}(p')\left[\gamma_\mu F_1(q^2) + i\sigma_{\mu\nu}q^\nu\frac{F_2(q^2)}{2m}\right]u(p), \tag{A28}$$

where F_1 and F_2 are the Pauli and Dirac form factors respectively, $q = p' - p$ with p' the momentum of the outgoing nucleon ($\bar{u}(p')$) and p the momentum of the incoming nucleon. For the Minkowski case, with our conventions we have

$$i\sigma_{\mu\nu}q^{\nu} = (q_\mu - \gamma_\mu \not{q}), \tag{A29}$$

and using the Dirac equation $(\not{p} - m)u = 0$ we get

$$\begin{aligned}&\bar{u}(p')[i\sigma_{\mu\nu}q^{\nu}]u(p)\\ &\quad = 2m\bar{u}(p')[\gamma_\mu]u(p) - \bar{u}(p')[p'_\mu + p_\mu]u(p).\end{aligned} \tag{A30}$$

On the other hand, with the Euclidean notation, we have $-\sigma^E_{\mu\nu}q^E_\nu = i(\gamma^E_\mu \not{q}^E - q^E_\mu)$. Similarly,

$$\begin{aligned}&\bar{u}^E(p'^E)[-\sigma^E_{\mu\nu}q^E_\nu]u^E(p^E)\\ &= 2m\bar{u}^E(p'^E)[\gamma^E_\mu]u^E(p) + i\bar{u}^E(p')[p'^E_\mu + p^E_\mu]u^E(p^E).\end{aligned} \tag{A31}$$

So in order to have consistent results for both Minkowski and Euclidean space, one should use $-\sigma^E_{\mu\nu}q^E_\nu$ under our convention,

$$\langle N'|\gamma_\mu|N\rangle^E = \bar{u}^E(p'^E)\left[\gamma^E_\mu F_1(q^2) - \sigma^E_{\mu\nu}q^E_\nu\frac{F_2(q^2)}{2m}\right]u^E(p^E). \tag{A32}$$

For the $\mathcal{CP}$ case, we have an additional form factor F'_3

$$-\sigma_{\mu\nu}q_\nu\gamma_5\frac{F'_3(q^2)}{2m}. \tag{A33}$$

N.B., when taking the phase carried by the $\mathcal{CP}$ spinors into consideration, this CP odd form factor should be modified as well. The relation between the correct $\mathcal{CP}$ form factor under the θ vacuum F_3 and F'_3 can be retrieved by considering the parity transformation of the normal spinors

$$u(p) \to u(\tilde{p}) = \gamma_4 u(p), \quad \bar{u}(p) \to \bar{u}(\tilde{p}) = \bar{u}(p)\gamma_4, \tag{A34}$$

and the $\mathcal{CP}$ ones

$$u^\theta(p) \to u^\theta(\tilde{p}) = e^{i\alpha_1\theta\gamma_5}\gamma_4 u(p) = (1 + i\alpha_1\theta\gamma_5)\gamma_4 u, \tag{A35}$$

$$\bar{u}^\theta(p) \to \bar{u}^\theta(\tilde{p}) = \bar{u}(p)\gamma_4 e^{i\alpha^1\theta\gamma_5} = \bar{u}(p)\gamma_4(1 + i\alpha_1\theta\gamma_5). \tag{A36}$$

Specifically, we have

$$i\theta F_3 = 2i\alpha^1\theta F_2 + i\theta F'_3 = i\theta(2\alpha^1 F_2 + F'_3). \tag{A37}$$

5. Correlation functions

In general, path integrals under the θ vacuum can be estimated by employing the Taylor expansion in θ and keeping only the leading term

$$\begin{aligned}&\int DA\cdot\mathrm{Det}[M]e^{-S_g + i\theta Q_t}\\ &\sim \int DA\cdot\mathrm{Det}[M]e^{-S_g} + i\theta\int DA\cdot\mathrm{Det}[M]Q_t e^{-S_g},\end{aligned} \tag{A38}$$

where $Q_t = \int d^4x q_t = \frac{g^2}{32\pi^2}\int d^4x F^E_{\mu\nu}\tilde{F}^{E,\mu\nu}$ is the total topological charge and q_t is the charge density. Correlation functions can therefore be accessed by

$${}_\theta\langle\ldots\rangle_\theta = \langle\ldots\rangle + i\theta\langle\ldots Q_t\rangle. \tag{A39}$$

For example, the two-point functions can be expressed as

$$G^\theta_2 = G_2 + i\theta G^Q_2, \tag{A40}$$

where G^θ_2, G_2, and G^Q_2 are two-point functions evaluated with the θ term, normal two-point functions, and two-point functions weighted by the topological charge, respectively. Since,

$$\begin{aligned}G^\theta_2 &= ZZ'^\dagger e^{-Et}\frac{m}{E}u^\theta(p)\bar{u}^\theta(p)\\ &= ZZ'^\dagger e^{-Et}\frac{m}{E}u\bar{u} + ZZ'^\dagger e^{-Et}\frac{m}{E}i\alpha^1\gamma_5\theta,\end{aligned} \tag{A41}$$

where Z and Z' are the sink and source overlapping factors and m and E are the nucleon mass and energy, and

$$G_2 = ZZ'^\dagger e^{-Et}\frac{m}{E}u(p)\bar{u}(p), \tag{A42}$$

we can get

$$G^Q_2 = G^\theta_2 - G_2 = ZZ'^\dagger e^{-Et}\frac{m}{E}\alpha^1\gamma_5. \tag{A43}$$

Here we are assuming t is large enough so that only the ground state survives to simplify the equations. These two-point correlation functions offer to a way of determining the $\mathcal{CP}$ angle α^1,

$$\frac{1}{2}\frac{\mathrm{Tr}[\gamma_5 G^Q_2]}{\mathrm{Tr}[\Gamma_e G_2]} = \frac{1}{2}\frac{\alpha^1\mathrm{Tr}[I_4]}{\frac{1}{2}\mathrm{Tr}[I_4]} = \alpha^1, \tag{A44}$$

where $\Gamma_e = \frac{1+\gamma_4}{2}$ is the unpolarized projector and I_4 is the 4 by 4 identity matrix. The angle α^1 is actually the leading

coefficient of the spinor dependence on θ, which, in some sense, measures the $\mathcal{CP}$ effect of the θ term.

For the three-point function case, similarly, we have

$$G_3^\theta = G_3 + i\theta G_3^Q. \tag{A45}$$

The normal three-point function is

$$G_3 = ZZ'^\dagger e^{-E_f(t_f-t_c)} e^{-E_i t_c} \frac{m^2}{E_f E_i} u(p_f)\langle N_f|J_\mu|N_i\rangle \bar{u}(p_i), \tag{A46}$$

where the subscripts i and f are for the initial and final nucleons respectively. Denoting the common factor $ZZ'^\dagger e^{-E_f(t_f-t_c)} e^{-E_i t_c} \frac{m^2}{E_f E_i} = A$ for simplicity, we have

$$G_3^\theta = A u^\theta(p_f)_\theta \langle N_f|J_\mu|N_i\rangle_\theta \bar{u}^\theta(p_i). \tag{A47}$$

The relation between the correlators and the form factors will be derived as follows. In general, the nucleon matrix elements in the three-point correlation functions can be decomposed into CP even and CP odd form factors W_μ^{even} and W_μ^{odd} as

$$G_3 = A u(p_f)\bar{u}(p_f) W_\mu^{\text{even}} u(p_i)\bar{u}(p_i), \tag{A48}$$

and

$$G_3^\theta = A u^\theta(p_f)\bar{u}^\theta(p_f)(W_\mu^{\text{even}} + i\theta W_\mu^{\text{odd}}) u^\theta(p_i)\bar{u}^\theta(p_i). \tag{A49}$$

Thus, we have

$$\frac{G_3}{A} = \left(\frac{-i\not{p}_f + m}{2m} W_\mu^{\text{even}} \frac{-i\not{p}_i + m}{2m}\right), \tag{A50}$$

and

$$\begin{aligned}\frac{G_3^\theta}{A} &= \frac{-i\not{p}_f + m e^{i2\alpha^1\theta\gamma_5}}{2m}(W_\mu^{\text{even}} + i\theta W_\mu^{\text{odd}}) \frac{-i\not{p}_i + m e^{i2\alpha^1\theta\gamma_5}}{2m} \\ &= \left(\frac{-i\not{p}_f + m}{2m} W_\mu^{\text{even}} \frac{-i\not{p}_i + m}{2m}\right) \\ &\quad + i\theta\left(\alpha^1\gamma_5 W_\mu^{\text{even}} \frac{-i\not{p}_i + m}{2m} + \frac{-i\not{p}_f + m}{2m} W_\mu^{\text{even}} \alpha^1\gamma_5 + \frac{-i\not{p}_f + m}{2m} W_\mu^{\text{odd}} \frac{-i\not{p}_i + m}{2m}\right).\end{aligned} \tag{A51}$$

So by doing a similar subtraction, we arrive at

$$\begin{aligned}\frac{G_3^Q}{A} &= \alpha^1\gamma_5 W_\mu^{\text{even}} \frac{-i\not{p}_i + m}{2m} + \frac{-i\not{p}_f + m}{2m} W_\mu^{\text{even}} \alpha^1\gamma_5 \\ &\quad + \frac{-i\not{p}_f + m}{2m} W_\mu^{\text{odd}} \frac{-i\not{p}_i + m}{2m}.\end{aligned} \tag{A52}$$

This is what the three-point correlator weighted by the topological charge looks like, and is what we use to extract the $\mathcal{CP}$ form factors.

APPENDIX B: EXTRACTING FORM FACTORS

To calculate the $\mathcal{CP}$ form factor, we need to the make three-point function to two-point function ratios

$$R_3(\Gamma_i, J_\mu) \equiv \frac{\text{Tr}[\Gamma_i G_3(J_\mu)]}{\text{Tr}[\Gamma_e G_2]} e^{E_f(t_f-t_c)} e^{E_i(t_c-t_0)}, \tag{B1}$$

and

$$R_3^Q(\Gamma_i, J_\mu) \equiv \frac{\text{Tr}[\Gamma_i G_3^Q(J_\mu)]}{\text{Tr}[\Gamma_e G_2]} e^{E_f(t_f-t_c)} e^{E_i(t_c-t_0)}, \tag{B2}$$

where Γ_i is the polarized projector and J_μ stands for the current insertion. If we write down the explicit form of the correlators, we have, e.g., in the CP even case,

$$R_3(\Gamma_i, J_\mu; \vec{p}_i, \vec{p}_f, \vec{p}) = \frac{\frac{m^2}{E_f E_i}\text{Tr}[\Gamma_i u(p_f)\langle N_f|J_\mu|N_i\rangle \bar{u}(p_i)]}{\frac{m}{E}\text{Tr}[\Gamma_e u(p)\bar{u}(p)]}. \tag{B3}$$

Here again we assume t is large enough to simplify the equations. Details of dealing with the excited-states contamination are discussed in the systematic uncertainty section, Sec. V. The additional overlapping and kinematic factors in Eqs. (B1) and (B2) are cancelled with proper combination of two-point correlation functions. Please note that in our numerical setup we always set the initial momentum $\vec{p_i} = 0$ in three-point functions. With proper selection of the momentum $\vec{p}_f$, polarization Γ_i and current insertion J_μ, the ratio gives the desired nucleon matrix element for particular form factors (or combinations of form factors). The relation between the corresponding form factors and the setup of the ratios are derived as follows.

For the normal EM case, we choose unpolarized projection and vector current γ_4, which gives (in our momentum setup)

$$\begin{aligned}R_3^{\text{EM1}}(\Gamma_e,\gamma_4) &= \frac{\text{Tr}[\Gamma_e G_3(\gamma_4)]}{\text{Tr}[\Gamma_e G_2(\vec{p}=0)]} \\ &= \frac{E_f+m}{2E_f}\left[F_1 - \frac{|\vec{q}|^2}{2m(E_f+m)}F_2\right] = \frac{E_f+m}{2E_f}G_E,\end{aligned}$$

where $G_E \equiv F_1 - \frac{q^2}{4m^2}F_2$ is the electric form factor. The last step used the fact that the momentum transfer

$$q^2 = |\vec{q}|^2 - \Delta E^2 = |\vec{q}|^2 - (E_f - m)^2 \tag{B4}$$

and

$$|\vec{q}|^2 = E_f^2 - m^2. \tag{B5}$$

Therefore, we have

$$q^2 = E_f^2 - m^2 - (E_f - m)^2 = \frac{2m}{E_f + m}|\vec{q}|^2, \tag{B6}$$

and

$$\frac{|\vec{q}|^2}{2m(E_f + m)} = \frac{1}{2m(E_f + m)}\frac{E_f + m}{2m}q^2 = \frac{q^2}{4m^2}. \tag{B7}$$

We can also choose polarized projection ($\Gamma_i \equiv -i\frac{1+\gamma_4}{2}\gamma_5\gamma_i$) and the γ_j current,

$$\begin{aligned} R_3^{\mathrm{EM2}}(\Gamma_i, \gamma_j) &= \frac{\mathrm{Tr}[\Gamma_i G_3(\gamma_j)]}{\mathrm{Tr}[\Gamma_e G_2(\vec{p}=0)]} \\ &= -\epsilon_{ijk}\frac{p_{f,k}}{2E_f}(F_1 + F_2) \\ &= -\epsilon_{ijk}\frac{p_{f,k}}{2E_f}G_M, \end{aligned} \tag{B8}$$

where $G_M \equiv F_1 + F_2$ is the magnetic form factor, or unpolarized projection and γ_i,

$$\begin{aligned} R_3^{\mathrm{EM3}}(\Gamma_e, \gamma_i) &= \frac{\mathrm{Tr}[\Gamma_e G_3(\gamma_i)]}{\mathrm{Tr}[\Gamma_e G_2(\vec{p}=0)]} \\ &= -i\frac{p_{f,i}}{2E_f}\left(F_1 - \frac{q^2}{4m^2}F_2\right) \\ &= -i\frac{p_{f,i}}{2E_f}G_E. \end{aligned}$$

These ratios can be used to extract the CP conserved form factors. For the $\not{C}\not{P}$ case, we can choose the polarized projection and γ_4, which turns out to be

$$\begin{aligned} R_3^{Q,\mathrm{EM1}}(\Gamma_i, \gamma_4) &= \frac{\mathrm{Tr}[\Gamma_i G_3^Q(\gamma_4)]}{\mathrm{Tr}[\Gamma_e G_2(\vec{p}=0)]} \\ &= \frac{p_{f,i}}{2E_f}\left[\alpha^1 F_1 + \frac{E_f + 3m}{2m}\alpha^1 F_2 + \frac{E_f + m}{2m}F_3'\right] \\ &= \frac{p_{f,i}}{2E_f}\left[\alpha^1 F_1 - \frac{E_f - m}{2m}\alpha^1 F_2 + \frac{E_f + m}{2m}(2\alpha^1 F_2 + F_3')\right] \\ &= \frac{p_{f,i}}{2E_f}\left[\alpha^1 G_E + \frac{E_f + m}{2m}F_3\right]. \end{aligned} \tag{B9}$$

An important fact about this ratio is that the neutron form factor $F_{3,n}(0)$ has no α^1 dependence since $G_{E,n}(0) = 0$. This means that one does not need to have any information about α^1 or the other CP-even form factors if one focuses only on the neutron case with $q^2 = 0$. But α^1 is still essential to obtain the correct values at nonzero q^2 for both the proton and neutron cases. Similarly, we can also use

$$\begin{aligned} R_3^{Q,\mathrm{EM2}}(\Gamma_i, \gamma_i) &= \frac{\mathrm{Tr}[\Gamma_i G_3^Q(\gamma_i)]}{\mathrm{Tr}[\Gamma_e G_2(\vec{p}=0)]} \\ &= -i\left[\alpha^1\frac{E_f - m}{2E_f}(F_1 + F_2) + \frac{p_{f,i}^2}{4mE_f}(\alpha^1 F_2 + F_3')\right] \\ &= -i\left[\alpha^1\frac{E_f - m}{2E_f}G_M + \frac{p_{f,i}^2}{4mE_f}(\alpha^1 F_2 + F_3')\right] \end{aligned}$$

and

$$R_3^{Q,\mathrm{EM3}}(\Gamma_i,\gamma_j) = \frac{\mathrm{Tr}[\Gamma_i G_3^Q(\gamma_j)]}{\mathrm{Tr}[\Gamma_e G_2(\vec{p}=0)]} = -\frac{i}{4}\left[\alpha^1 \frac{p_{f,i}p_{f,j}}{mE_f}F_2 + \frac{p_{f,i}p_{f,j}}{mE_f}F_3'\right] = -\frac{i}{4}\frac{p_{f,i}p_{f,j}}{mE_f}[\alpha^1 F_2 + F_3'], \tag{B10}$$

which prefers giving the combination of $\alpha^1 F_2 + F_3'$ rather than $F_3 = 2\alpha^1 F_2 + F_3'$.

We use the ratios $R_3^{\mathrm{EM1}}(\Gamma_e,\gamma_4)$, $R_3^{\mathrm{EM2}}(\Gamma_i,\gamma_j)$, and $R_3^{Q,\mathrm{EM1}}(\Gamma_i,\gamma_4)$ in our calculation.

[1] A. D. Sakharov, Violation of *CP* invariance, C asymmetry, and baryon asymmetry of the universe, Sov. Phys. Usp. **34**, 392 (1991).

[2] Glennys R. Farrar and M. E. Shaposhnikov, Baryon asymmetry of the universe in the minimal Standard Model, Phys. Rev. Lett. **70**, 2833 (1993); **71**, 210(E) (1993).

[3] Glennys R. Farrar and M. E. Shaposhnikov, Baryon asymmetry of the universe in the standard electroweak theory, Phys. Rev. D **50**, 774 (1994).

[4] M. B. Gavela, P. Hernandez, J. Orloff, and O. Pene, Standard model *CP* violation and baryon asymmetry, Mod. Phys. Lett. A **9**, 795 (1994).

[5] M. B. Gavela, P. Hernandez, J. Orloff, O. Pene, and C. Quimbay, Standard model *CP* violation and baryon asymmetry. Part 2: Finite temperature, Nucl. Phys. **B430**, 382 (1994).

[6] Patrick Huet and Eric Sather, Electroweak baryogenesis and Standard Model *CP* violation, Phys. Rev. D **51**, 379 (1995).

[7] J. H. Smith, E. M. Purcell, and N. F. Ramsey, Experimental limit to the electric dipole moment of the neutron, Phys. Rev. **108**, 120 (1957).

[8] C. Abel *et al.*, Measurement of the permanent electric dipole moment of the neutron, Phys. Rev. Lett. **124**, 081803 (2020).

[9] M. Abramczyk, S. Aoki, T. Blum, T. Izubuchi, H. Ohki, and S. Syritsyn, Lattice calculation of electric dipole moments and form factors of the nucleon, Phys. Rev. D **96**, 014501 (2017).

[10] E. Shintani, S. Aoki, N. Ishizuka, K. Kanaya, Y. Kikukawa, Y. Kuramashi, M. Okawa, Y. Tanigchi, A. Ukawa, and T. Yoshie, Neutron electric dipole moment from lattice QCD, Phys. Rev. D **72**, 014504 (2005).

[11] F. Berruto, T. Blum, K. Orginos, and A. Soni, Calculation of the neutron electric dipole moment with two dynamical flavors of domain wall fermions, Phys. Rev. D **73**, 054509 (2006).

[12] F. K. Guo, R. Horsley, U. G. Meissner, Y. Nakamura, H. Perlt, P. E. L. Rakow, G. Schierholz, A. Schiller, and J. M. Zanotti, The electric dipole moment of the neutron from $2+1$ flavor lattice QCD, Phys. Rev. Lett. **115**, 062001 (2015).

[13] Eigo Shintani, Thomas Blum, Taku Izubuchi, and Amarjit Soni, Neutron and proton electric dipole moments from $N_f = 2+1$ domain-wall fermion lattice QCD, Phys. Rev. D **93**, 094503 (2016).

[14] C. Alexandrou, A. Athenodorou, M. Constantinou, K. Hadjiyiannakou, K. Jansen, G. Koutsou, K. Ottnad, and M. Petschlies, Neutron electric dipole moment using $N_f = 2+1+1$ twisted mass fermions, Phys. Rev. D **93**, 074503 (2016).

[15] Sergey Syritsyn, Taku Izubuchi, and Hiroshi Ohki, Calculation of nucleon electric dipole moments induced by quark chromo-electric dipole moments and the QCD θ-term, Proc. Sci. Confinement2018 (**2019**) 194.

[16] Jack Dragos, Thomas Luu, Andrea Shindler, Jordy de Vries, and Ahmed Yousif, Confirming the existence of the strong *CP* problem in lattice QCD with the gradient flow, Phys. Rev. C **103**, 015202 (2021).

[17] C. Alexandrou, A. Athenodorou, K. Hadjiyiannakou, and A. Todaro, Neutron electric dipole moment using lattice QCD simulations at the physical point, Phys. Rev. D **103**, 054501 (2021).

[18] Tanmoy Bhattacharya, Vincenzo Cirigliano, Rajan Gupta, Emanuele Mereghetti, and Boram Yoon, Contribution of the QCD Θ-term to the nucleon electric dipole moment, Phys. Rev. D **103**, 114507 (2021).

[19] Keh-Fei Liu, Jian Liang, and Yi-Bo Yang, Variance reduction and cluster decomposition, Phys. Rev. D **97**, 034507 (2018).

[20] Varouzhan Baluni, *CP* violating effects in QCD, Phys. Rev. D **19**, 2227 (1979).

[21] Y. Aoki *et al.*, Continuum limit physics from $2+1$ flavor domain wall QCD, Phys. Rev. D **83**, 074508 (2011).

[22] Herbert Neuberger, Exactly massless quarks on the lattice, Phys. Lett. B **417**, 141 (1998).

[23] P. Hasenfratz, S. Hauswirth, T. Jorg, F. Niedermayer, and K. Holland, Testing the fixed point QCD action and the construction of chiral currents, Nucl. Phys. **B643**, 280 (2002).

[24] A. Li *et al.*, Overlap valence on $2+1$ flavor domain wall fermion configurations with deflation and low-mode substitution, Phys. Rev. D **82**, 114501 (2010).

[25] Yi-Bo Yang, Andrei Alexandru, Terrence Draper, Ming Gong, and Keh-Fei Liu, Stochastic method with low mode substitution for nucleon isovector matrix elements, Phys. Rev. D **93**, 034503 (2016).

[26] Keh-Fei Liu, Heavy and light quarks with lattice chiral fermions, Int. J. Mod. Phys. A **20**, 7241 (2005).

[27] Jian Liang, Yi-Bo Yang, Terrence Draper, Ming Gong, and Keh-Fei Liu, Quark spins and anomalous ward identity, Phys. Rev. D **98**, 074505 (2018).

[28] M. Müller-Preussker, Recent results on topology on the lattice (in memory of Pierre van Baal), Proc. Sci. LATTICE2014 (**2015**) 003.
[29] Martin Lüscher, Properties and uses of the Wilson flow in lattice QCD, J. High Energy Phys. 08 (2010) 071.
[30] Martin Luscher and Peter Weisz, Perturbative analysis of the gradient flow in non-Abelian gauge theories, J. High Energy Phys. 02 (2011) 051.
[31] Martin Luscher, Chiral symmetry and the Yang–Mills gradient flow, J. High Energy Phys. 04 (2013) 123.
[32] David H. Adams, Axial anomaly and topological charge in lattice gauge theory with overlap Dirac operator, Ann. Phys. (Berlin) **296**, 131 (2002).
[33] Kazuo Fujikawa, A continuum limit of the chiral Jacobian in lattice gauge theory, Nucl. Phys. **B546**, 480 (1999).
[34] Donal O'Connell and Martin J. Savage, Extrapolation formulas for neutron EDM calculations in lattice QCD, Phys. Lett. B **633**, 319 (2006).
[35] One way to understand this is to think of the nucleon two-point function. The term $i\theta \mathrm{Tr}[\frac{1+\gamma_4}{2}\langle \chi Q_t \bar{\chi}\rangle]$ vanishes due to the 0^{-+} quantum number of Q_t.